BLIND NONLINEAR UNMIXING FOR INTIMATE MIXTURES USING HAPKE MODEL AND CNN

Behnood Rasti[1], and Bikram Koirala[2],

[1] Helmholtz-Zentrum Dresden-Rossendorf (HZDR), Helmholtz Institute Freiberg for Resource Technology.
[2] Imec-Visionlab, University of Antwerp (CDE) Universiteitsplein 1, B-2610 Antwerp

ABSTRACT

We propose a blind nonlinear unmixing technique for intimate mixtures. We use the Hapke model and a fully convolutional neural networks (HapkeCNN). The proposed loss function contains 1) A quadratic term based on the Hapke model, 2) reconstruction error, and 3) a minimum volume term. The first term captures the nonlinearity, the second ensures the fidelity of the reconstructed reflectance, and the latter term exploits the geometrical information. The proposed method is evaluated using a simulated and a real datasets. We compare the results of endmember and abundance estimation with bilinear, multilinear, nonlinear, and projection-based linear unmixing techniques. The experimental results confirm that HapkeCNN considerably outperforms the state-of-the-art nonlinear approaches in terms of spectral angle distance and root mean square error. HapkeCNN was implemented in Python (3.9) using PyTorch as the platform for the deep network and is available online: https://github.com/BehnoodRasti/HapkeCNN.

Index Terms— Hyperspectral image, nonlinear unmixing, convolutional neural network, albedo, deep learning, Hapke model, endmember estimation, minimum simplex volume, blind unmixing

1. INTRODUCTION

Hyperspectral sensors capture the spectral signature of materials in a range of wavelength. The measured spectra are generally mixtures of pure spectra of the materials within the pixels. Therefore, the observed spectra can be modeled using a mixing model. A mixing model assumes that the observed spectral pixel can be modeled using a few spectra called endmembers corresponding to the pure spectra of the materials existing in that pixel. As a result, the endmembers are associated with abundance fractions within that pixel's area. Unmixing is the task of estimating the fractional abundances of the endmembers within spectral pixels, which often relies on estimating or extracting the endmembers. The abundances are nonnegative and have to sum to one forming two main constraints so-called abundance nonnegativity constraint (ANC) and abundance sum-to-one constraint (ASC), respectively. In blind unmixing both endmembers and abundances are estimated simultaneously. Alternatively, endmembers can be extracted before the abundance estimation using geometrical assumptions [1].

The mixing model is either linear or nonlinear. In linear unmixing, the endmembers are assumed to be linearly mixed. The linear model is valid when each light ray only interacts with one material before reaching the sensor. This is a common assumption in Earth observation applications, due to the macroscopic problems at hand. On the other hand, the linear approximation often fails in the case of intimate mixtures and when the light undergoes multiple reflections before reaching the sensor. In that case, nonlinear models must be utilized [1, 2].

This paper proposes a blind nonlinear unmixing method using the Hapke model and convolutional neural networks (HapkeCNN). HapkeCNN simultaneously estimates the endmembers and abundances by relying on the linear mixture assumption of the albedos. The proposed loss function exploits a total variation-based minimum simplex volume term, which helps to estimate endmembers in the absence of pure spectral pixels, using geometrical information [3, 4].

1.1. Hyperspectral Modeling Using the Hapke model

We use the simplified Hapke model i.e.,

$$\mathbf{Y} \quad = \quad F(\mathbf{A}, \mathbf{E}) \tag{1}$$

where $\mathbf{Y} \in \mathbb{R}^{p \times n}$ is the observed data, $\mathbf{E} \in \mathbb{R}^{p \times r}$, and $\mathbf{A} \in \mathbb{R}^{r \times n}$, $r \ll p$ contain the r endmembers and fractional abundances, respectively.

The Hapke model assumes that the single-scattering albedos (SSA) of pure materials ($\mathbf{W} = R^{-1}(\mathbf{E}) \in \mathbb{R}^{p \times r}$, $r \ll p$) are mixed linearly:

$$\mathbf{X} = \mathbf{W}\mathbf{A}, \ \text{s.t.} \ \mathbf{A} \geq 0, \mathbf{1}_r^T \mathbf{A} = \mathbf{1}_n^T, 0 \leq \mathbf{W} \leq 1, \tag{2}$$

where $\mathbf{X} = R^{-1}(\mathbf{Y}) \in \mathbb{R}^{p \times n}$ contains the albedos of the observed reflectances. $\mathbf{1}_n$ indicates an n-component column vector of ones. In this work, we propose the following model

$$\begin{aligned} \mathbf{Y} =& R(R^{-1}(\mathbf{E})\mathbf{A}) + \mathbf{N}, \\ & \text{s.t.} \ \mathbf{A} \geq 0, \mathbf{1}_r^T \mathbf{A} = \mathbf{1}_n^T, 0 \leq \mathbf{E} \leq 1, \end{aligned} \tag{3}$$

where $\mathbf{N} \in \mathbb{R}^{p \times n}$ is noise.

We use a fully convolutional neural network with a skip connection to estimate $\mathbf{E}$ and $\mathbf{A}$, simultaneously. Fig. 1 shows the proposed CNN used for the abundance and endmember estimation. The deep network proposed in this work utilizes five well-established CNN modules shown in purple color, which include a convolutional layer (Conv), batch normalization (BN), and an activation function. The BN layers speed up the learning process and provide more robustness for selecting the hyperparameters. We use Leaky ReLU (rectified linear unit) as the nonlinear activation function for all CNN modules. We use the softmax activation function to enforce both the ASC and ANC. The final convolutional layer is used with the same number of filters as the number of endmember. The endmembers are the weights of the final convolutional layer. The skip connection can easily learn the identity function and therefore avoids vanishing gradients in a deep network. Table 1 depicts the hyperparameters used in HapkeCNN. We set the number of iterations to 8000 and use

Table 1. Hyperparameters used for HapkeCNN.

Hyperparameters				
	Input Ch.	Ouput Ch.	Filter Size	Stride
Conv1	p	256	3x3	2
Conv2	256	256	3x3	1
Conv3	260	256	3x3	1
Conv4	256	256	3x3	1
Conv5	256	r	3x3	1
Conv6	r	p	1x1	1
ConvSkip	p	4	1x1	1
	Negative Slope			
Leaky ReLU	0.1			
	Scale Factor		Mode	
Upsample	2		Bilinear	
	Type	Learning Rate		Iterations
Optimizer	Adam	0.001		8000

exponentially weighted averaging over the outputs to make the algorithm robust to the variance of the loss function at the stopping point. Adam optimizer is used with a learning rate of 0.001 to minimize the loss function. The loss consists of three terms given by

$$\mathcal{L}(\mathbf{Y}, \hat{\mathbf{Y}}, \mathbf{A}, \mathbf{E}) = \frac{1}{2}||\mathbf{Y} - R(R^{-1}(\mathbf{E})\mathbf{A})||_F^2 + \frac{\alpha}{2}||\mathbf{Y} - \hat{\mathbf{Y}}||_F^2 + \lambda TV(R^{-1}(\mathbf{E})) \quad (4)$$

where $\|.\|_F$ denotes the Frobenius norm. The first term uses the proposed model given in (3) to capture the nonlinearity of the data. The second term minimizes the reconstruction error of input reflectances and the reconstructed ones. The third term is a geometrical total variation penalty which enforces the data simplex to have the minimum volume [5]. Assuming $\mathbf{W} = R^{-1}(\mathbf{E})$ the total variation geometrical penalty is given by [5, 3]

$$TV(\mathbf{W}) = \sum_{i,j=1}^{r} \frac{1}{2}||\mathbf{w}_i - \mathbf{w}_j||_2^2 = \sum_{i=1}^{r} ||\mathbf{w}_i - \frac{1}{r}\mathbf{W}\mathbf{1}_r||_2^2 = ||\mathbf{W}(\mathbf{I}_r - \frac{1}{r}\mathbf{1}_r\mathbf{1}_r^T)||_F^2 \quad (5)$$

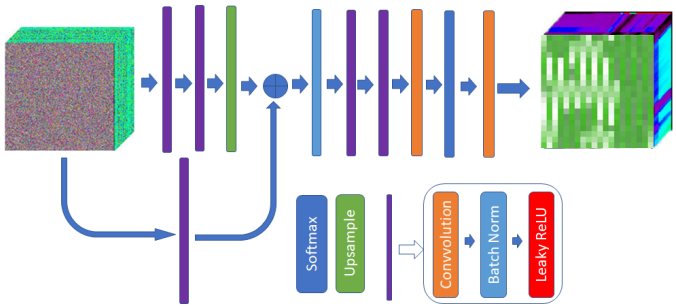

Fig. 1. The architecture of HapkeCNN. HapkeCNN uses a CNN with a skip connection and six convolutional layers. The softmax layer generates the abundances and the endmembers are the weights of the final convolutional.

2. EXPERIMENTS

2.1. The Data

2.1.1. Simulated Data

The hyperspectral dataset of 105×105 pixels is simulated by combining six endmembers (Fig. 2(b)) nonlinearly. The Hapke model is chosen as a nonlinear mixing model. This dataset does not have pure pixels, but at least two nonlinearly mixed data points are available on each facet of the nonlinear data manifold to geometrically reconstruct virtual endmembers (see [4] for geometrical demonstration).

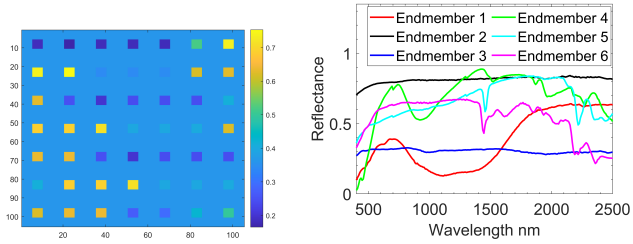

(a) (b)

Fig. 2. Simulated Dataset: a) Band number 70 (1050 nm) b) Endmembers.

2.1.2. *Real Data: RELAB dataset*

This hyperspectral image of 60×60 pixels (see Fig. 3 (a)) is generated by utilizing the real spectral reflectance of mineral mixtures. In total, there are nine unique spectral reflectances in this image. These nine spectra were acquired in the NASA Reflectance Experiment Laboratory (RELAB) at Brown University ([6]) by mixing three minerals (Anorthite (An), Bronzite (Br) and Olivine (Ol)). The spectral reflectances of these three minerals are shown in Fig. 3 (b). Each spectral reflectance contains reflection values for 461 different spectral bands covering the wavelength region [300-2600] nm. These three minerals have equivalent grain sizes and densities, making the areal and volumetric fractional abundances identical. The size of the particles (of the order of 100 μm) is much larger than the wavelength of the light. We like to mention that all nine mixtures are binary mixtures, i.e., the mixture of An-Br, the mixture of Br-Ol, and the mixture of An-Ol. For each mineral pair, the spectra of three mixtures (0.75/0.25, 0.5/0.5, and 0.25/0.75) are available. In the experimental part, we will demonstrate that these nine unique spectra are sufficient to geometrically reconstruct the virtual endmembers. These nine spectra were selected because the Hapke model can accurately estimate the fractional abundances of these mixtures.

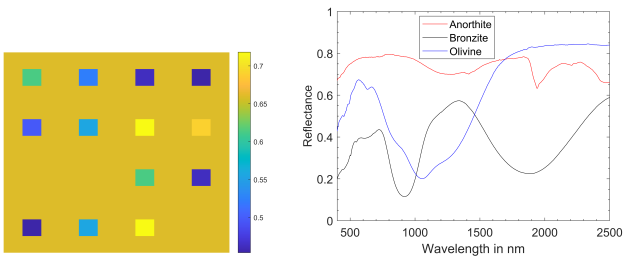

(a) (b)

Fig. 3. Relab Dataset 1: a) Band number 250 (1545 nm) b) Endmembers.

2.2. Experimental Setup

Six unmixing techniques from different unmixing categories were used as competing methods in the experiments: Geometrical unmixing: FCLSU [7] using VCA [8] for endmember extraction. Geometrical and blind unmixing: NMF-QMV [3]. Blind unmixing is performed in the single scattering albedo space (i.e., the linear space). Bilinear unmixing: PPNM [9] using VCA [8] for endmember extraction. Multilinear unmixing: MLM [10] using VCA [8] for endmember extraction (same endmembers used by PPNM). Nonnegative Tensor Factorization: LR-NTF [11] using VCA [8] for endmember extraction (same endmembers used by PPNM). Deep unmixing method: UnDIP [12] using SiVM [13] for endmember extraction. Endmember extraction and abundance estimation is performed in the single scattering albedo space. For FCLSU, the unmixing is performed in the albedo space. Note that for NMF-QMV, we choose the "TV" as the optional penalty term. For the Hapke model, we set parameters $\mu_0 = 1$ and $\mu = 1$. For HapkeCNN we set $\alpha = 0.0001$ and $\lambda = 0.1$. Additionally, we project the dataset into a subspace to reduce the noise effect. We choose all the parameters for the competing methods according to the reported default values.

2.3. Unmixing Experiments

2.3.1. *Simulated Dataset*

Table 2 and 3 give the abundance RMSE and SAD for all unmixing methods applied to simulated dataset. The unmixing results confirm substantial improvements of HapkeCNN for all cases. The other unmixing techniques cannot cope with the absence of pure pixels. Although NMF-QMV is designed for such scenarios, the nonlinear transformation considerably weakens its performance. Fig. 4 and 5 compare the estimated abundances and endmembers obtained by applying different unmixing techniques to the Simulated dataset for 40 dB SNR.

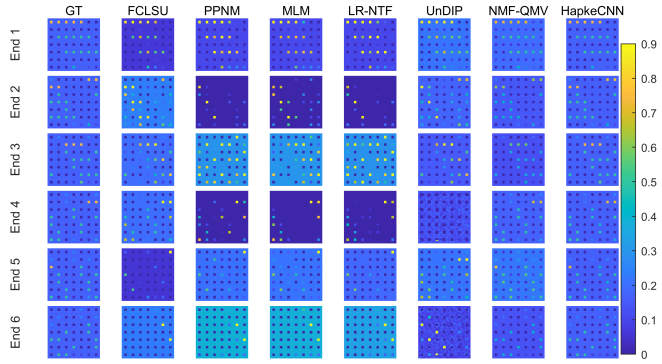

Fig. 4. Simulated dataset (40dB) - The visual comparison of the abundance maps obtained by applying different unmixing techniques.

2.3.2. *Real Dataset*

The unmixing results for the Relab dataset are given in Table 4 and 5 in terms of abundance RMSE and SAD, respectively. HapkeCNN significantly outperforms the other techniques in terms of RMSE and SAD, and NMF-QMV provides the second-best results. The other methods show poor performances. Additionally, HapkeCNN shows robustness in terms of noise power, while NMF-QMV shows poor performance in the very noisy scenario, i.e., 20 dB. Fig. 6 and 7 visually compare the performance of the unmixing technique applied to the Relab dataset for 40 dB SNR. The visual comparison

Table 2. RMSE (Simulated dataset). The best performances are shown in bold.

	FCLSU	PPNM	MLM	LR-NTF	UnDIP	NMF-QMV	HapkeCNN
20dB	21.57±3.07	23.62±5.05	22.71±5.83	25.07±5.48	10.08±0.65	12.54±1.4	**4.69±0.06**
30dB	18.74±1.72	20.24±1.71	19.92±2.12	20.23±1.78	10.3±0.48	7.71±1	**1.67±0.02**
40dB	14.68±1.62	18.63±2.36	17.05±2.49	18.16±2.63	8.48±1.6	3.13±1.26	**0.76±0.16**
50dB	11.53±2.26	17.9±3	16.02±2.15	17.12±4.13	7.24±0.15	3.36±1.88	**0.52±0.01**

Table 3. SAD (Simulated dataset). The best performances are shown in bold.

	SiVM	VCA	NMF-QMV	HapkeCNN
20dB	9.49±0.27	13.26±2.44	10.85±2.08	**2.08±0.04**
30dB	6.8±0.47	9.25±1.27	4.6±1.06	**1.06±0.02**
40dB	6.49±0.32	7.2±1.58	3.14±1.51	**1.51±0.02**
50dB	5.8±0.01	5.33±1.14	3.13±1.76	**1.76±0.01**

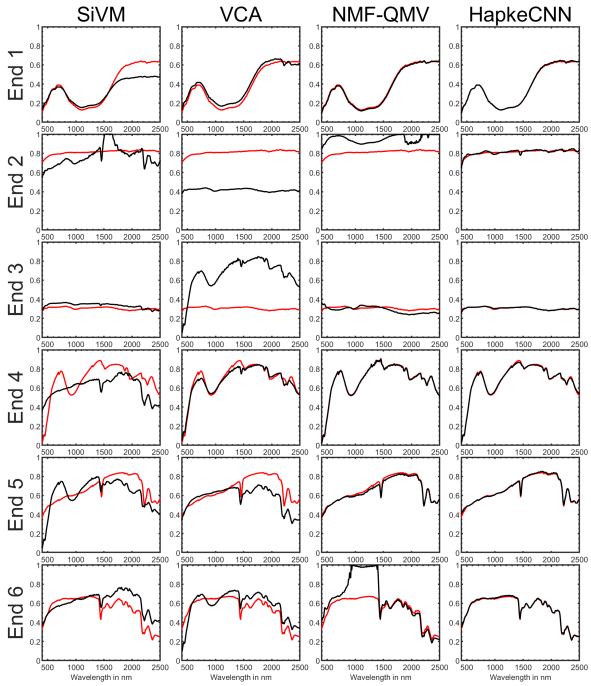

Fig. 5. Simulated dataset (40dB) - The visual comparison of the endmembers obtained by applying different unmixing techniques. Red: the ground truth endmembers; Black: the estimated endmembers.

reveals that HapkeCNN considerably outperforms the other methods for both endmember and abundance estimation.

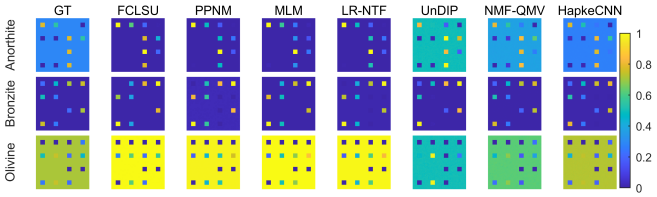

Fig. 6. Relab dataset (40dB) - The visual comparison of the abundance maps obtained by applying different unmixing techniques.

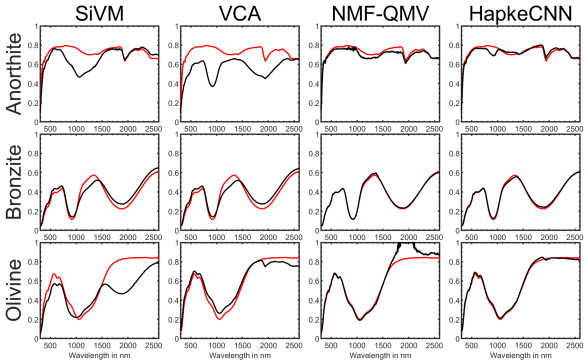

Fig. 7. Relab dataset (40dB) - The visual comparison of the endmembers obtained by applying different unmixing techniques. Red: the ground truth endmembers; Black: the estimated endmembers.

3. CONCLUSIONS

We proposed a blind nonlinear unmixing technique for the intimate mixtures using the Hapke model and CNN (HapkeCNN). HapkeCNN estimates both endmembers and abundances simultaneously using a novel loss function. The performance of HapkeCNN applied to a real and a simulated dataset was compared with the other nonlinear methods. The results confirmed that HapkeCNN considerably outperforms the other techniques. Additionally, the experiments revealed

Table 4. RMSE (Relab). The best performances are shown in bold.

	FCLSU	PPNM	MLM	LR-NTF	UnDIP	NMF-QMV	HapkeCNN
20dB	20.73±1.64	21.97±6.71	20.11±8.86	20.83±7.56	29.58±4.62	20.32±1.49	**1.94±0.09**
30dB	15.77±1.08	16.89±4.21	11.91±3.67	14.85±2.17	17.62±1.79	8.86±1	**1.39±0.23**
40dB	20.41±2.03	21.04±2.55	20.03±4.5	22.68±3.71	16.92±0.21	6.72±0.38	**1.58±0.17**
50dB	20.76±2.98	20.66±3.97	19.51±6.71	24.79±4.38	16.82±0.06	6.2±0.28	**1.54±0.14**

Table 5. SAD (Relab). The best performances are shown in bold.

	SiVM	VCA	NMF-QMV	HapkeCNN
20dB	10.8±1.91	16.12±3.61	10.68±1.14	**1.67±0.1**
30dB	6.61±0.94	13.04±0.67	3.7±0.97	**1.57±0.07**
40dB	6.94±0.63	13.4±0.03	2.29±0.26	**1.61±0.05**
50dB	7.25±0.85	13.5±0.01	2.06±0.28	**1.58±0.05**

that HapkeCNN successfully estimates virtual endmembers in the absence of pure pixels, and it is robust to noise.

4. REFERENCES

[1] J. M. Bioucas-Dias, A. Plaza, N. Dobigeon, M. Parente, Q. Du, P. Gader, and J. Chanussot, "Hyperspectral unmixing overview: Geometrical, statistical, and sparse regression-based approaches," *IEEE J. Sel. Topics Appl. Earth Observ. Remote Sens.*, vol. 5, no. 2, pp. 354–379, April 2012.

[2] N. Dobigeon, J. Tourneret, C. Richard, J. C. M. Bermudez, S. McLaughlin, and A. O. Hero, "Nonlinear unmixing of hyperspectral images: Models and algorithms," *IEEE Signal Processing Magazine*, vol. 31, no. 1, pp. 82–94, 2014.

[3] L. Zhuang, C. Lin, M. A. T. Figueiredo, and J. M. Bioucas-Dias, "Regularization parameter selection in minimum volume hyperspectral unmixing," *IEEE Transactions on Geoscience and Remote Sensing*, vol. 57, no. 12, pp. 9858–9877, 2019.

[4] B. Rasti, B. Koirala, P. Scheunders, and J. Chanussot, "Misicnet: Minimum simplex convolutional network for deep hyperspectral unmixing," *IEEE Transactions on Geoscience and Remote Sensing*, vol. 60, pp. 1–15, 2022.

[5] M. Berman, H. Kiiveri, R. Lagerstrom, A. Ernst, R. Dunne, and J.F. Huntington, "Ice: a statistical approach to identifying endmembers in hyperspectral images," *IEEE Transactions on Geoscience and Remote Sensing*, vol. 42, no. 10, pp. 2085–2095, 2004.

[6] J. F. Mustard and C. M. Pieters, "Photometric phase functions of common geologic minerals and applications to quantitative analysis of mineral mixture reflectance spectra," *Journal of Geophysical Research*, vol. 94, pp. 13619–13634, 1989.

[7] D. C. Heinz and Chein-I-Chang, "Fully constrained least squares linear spectral mixture analysis method for material quantification in hyperspectral imagery," *IEEE Transactions on Geoscience and Remote Sensing*, vol. 39, no. 3, pp. 529–545, 2001.

[8] J. Nascimento and J. Bioucas-Dias, "Vertex component analysis: A˜fast algorithm to extract endmembers spectra from hyperspectral data," in *Pattern Recognition and Image Analysis*, Francisco José Perales, Aurélio J. C. Campilho, Nicolás Pérez de la Blanca, and Alberto Sanfeliu, Eds., Berlin, Heidelberg, 2003, pp. 626–635, Springer Berlin Heidelberg.

[9] W. Fan, B. Hu, J. Miller, and M. Li, "Comparative study between a new nonlinear model and common linear model for analysing laboratory simulated-forest hyperspectral data," *International Journal of Remote Sensing*, vol. 30, no. 11, pp. 2951–2962, 2009.

[10] R. Heylen and P. Scheunders, "A multilinear mixing model for nonlinear spectral unmixing," *IEEE Transactions on Geoscience and Remote Sensing*, vol. 54, no. 1, pp. 240–251, Jan 2016.

[11] L. Gao, Z. Wang, L. Zhuang, H. Yu, B. Zhang, and J. Chanussot, "Using low-rank representation of abundance maps and nonnegative tensor factorization for hyperspectral nonlinear unmixing," *IEEE Transactions on Geoscience and Remote Sensing*, vol. 60, pp. 1–17, 2022.

[12] B. Rasti, B. Koirala, P. Scheunders, and P. Ghamisi, "UnDIP: Hyperspectral unmixing using deep image prior," *IEEE Transactions on Geoscience and Remote Sensing*, pp. 1–15, 2021.

[13] R. Heylen, D. Burazerovic, and P. Scheunders, "Fully constrained least squares spectral unmixing by simplex projection," *IEEE Transactions on Geoscience and Remote Sensing*, vol. 49, no. 11, pp. 4112–4122, Nov 2011.